Journal of Molecular Graphics and Modelling 32 (2012) 39–48

Contents lists available at SciVerse ScienceDirect

Journal of Molecular Graphics and Modelling

journal homepage: www.elsevier.com/locate/JMGM

Study of differences in the VEGFR2 inhibitory activities between semaxanib and SU5205 using 3D-QSAR, docking, and molecular dynamics simulations

Camila Muñoz[a], Francisco Adasme[a], Jans H. Alzate-Morales[a], Ariela Vergara-Jaque[a], Torsten Kniess[b], Julio Caballero[a,*]

[a] Centro de Bioinformática y Simulación Molecular, Universidad de Talca, 2 Norte 685, Casilla 721, Talca, Chile
[b] Institute of Radiopharmacy, Helmholtz-Zentrum, Dresden-Rossendorf e.V., PO Box 510119, D-01314 Dresden, Germany

ARTICLE INFO

Article history:
Received 5 August 2011
Received in revised form
30 September 2011
Accepted 15 October 2011
Available online 20 October 2011

Keywords:
VEGFR2
Semaxanib
CoMFA
Docking
Molecular dynamics
MM-GBSA

ABSTRACT

Semaxanib (SU5416) and 3-[4′-fluorobenzylidene]indolin-2-one (SU5205) are structurally similar drugs that are able to inhibit vascular endothelial growth factor receptor-2 (VEGFR2), but the former is 87 times more effective than the latter. Previously, SU5205 was used as a radiolabelled inhibitor (as surrogate for SU5416) and a radiotracer for positron emission tomography (PET) imaging, but the compound exhibited poor stability and only a moderate IC_{50} toward VEGFR2. In the current work, the relationship between the structure and activity of these drugs as VEGFR2 inhibitors was studied using 3D-QSAR, docking and molecular dynamics (MD) simulations. First, comparative molecular field analysis (CoMFA) was performed using 48 2-indolinone derivatives and their VEGFR2 inhibitory activities. The best CoMFA model was carried out over a training set including 40 compounds, and it included steric and electrostatic fields. In addition, this model gave satisfactory cross-validation results and adequately predicted 8 compounds contained in the test set. The plots of the CoMFA fields could explain the structural differences between semaxanib and SU5205. Docking and molecular dynamics simulations showed that both molecules have the same orientation and dynamics inside the VEGFR2 active site. However, the hydrophobic pocket of VEGFR2 was more exposed to the solvent media when it was complexed with SU5205. An energetic analysis, including Embrace and MM-GBSA calculations, revealed that the potency of ligand binding is governed by van der Waals contacts.

1. Introduction

Semaxanib (or SU5416) is a potent and selective inhibitor of the vascular endothelial growth factor receptor-2 (VEGFR2) tyrosine kinase [1]. Inhibition of VEGFR2 blocks signal transduction of the VEGF pathway, thereby affecting many of the processes involved in tumor growth, progression, metastasis, and angiogenesis [2]. Therefore, semaxanib has been studied for use in antiangiogenic therapies.

Positron emission tomography (PET) is a nuclear medicine imaging technique that allows for visualization of specific targets on the molecular level [3]. Monitoring the antiangiogenic effects of a compound is an important step toward clinical trials for a potential cancer treatment. Direct, noninvasive molecular imaging of angiogenesis allows for an adequate selection of patients for antiangiogenesis therapy and a better assessment of the efficacy of treatments that target angiogenesis. The development of small molecule tyrosine kinase inhibitors labeled with the short-lived positron emitters represents an attractive basis for monitoring the overexpression of VEGFR2 tyrosine kinases. Fluorine-18 is the most frequently used radionuclide in PET imaging due to its excellent physical characteristics for imaging. The half-life of ^{18}F is 109.8 min, which allows for complex radiosynthesis reactions and extended pharmacological *in vivo* studies.

Recently, one of the authors of the present study (Kniess) and his co-workers used semaxanib as a lead structure for the development of an ^{18}F-labeled radiotracer [4]. The introduction of the radionuclide into the oxindole core as well into the pyrrole core of semaxanib was unsuccessful; therefore, the authors developed 3-[4′-fluorobenzylidene]indolin-2-one (SU5205) as a surrogate for semaxanib by substitution of the dimethylpyrrol moiety with a 4-fluoro-phenyl ring (Fig. 1). SU5205 was found not to be a suitable radiotracer for imaging receptor tyrosine kinases due to its poor stability and its only moderate IC_{50} affinity for VEGFR2 [4].

The design of a derivative compound based on the structure of oxindole with sub-nanomolar affinity for VEGFR2 similar to that of the original structure of semaxanib is desirable. For this purpose, knowledge of the relevant structural features that positively

* Corresponding author. Tel.: +56 71 201 685; fax: +56 71 201 662.
E-mail addresses: jmcr77@yahoo.com, jcaballero@utalca.cl (J. Caballero).

1093-3263/$ – see front matter © 2011 Elsevier Inc. All rights reserved.
doi:10.1016/j.jmgm.2011.10.005

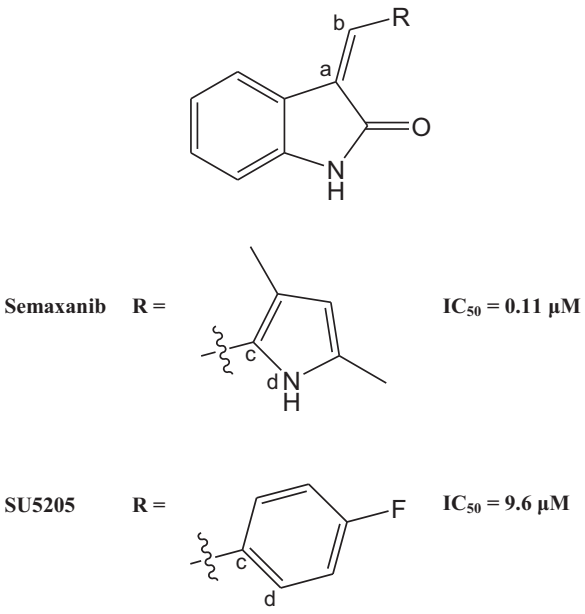

Fig. 1. The structures of semaxanib and SU5205. The atoms involved in the torsional angle φ are labeled.

influence the activity of VEGFR2 and that affect the molecular interactions between VEGFR2 and its inhibitors would be useful. The atomistic analysis of enzyme–inhibitor complexes can be carried out with structural bioinformatics methods. Models that are able to explain the interactions and predict the biological activity of compounds based on their structural properties are considered powerful tools to design highly active kinase inhibitors. Computational methods, such as docking [5–7], quantitative structure–activity relationship (QSAR) [7–13], pharmacophore modeling [14,15], de novo design [16,17], quantum mechanics/molecular mechanics (QM/MM) [5,13,18–20], and molecular dynamics (MD) [21], have been used to study kinase inhibitors. In the recent literature, there are several reports that carried out computational studies on VEGFR2 inhibitors. Most of these studies combined molecular docking and three dimensional (3D) QSAR to understand the structure–activity correlation of VEGFR2 inhibitors [22–24]. In a recent paper, Li et al. [25] developed a predictive nonlinear QSAR model for the inhibition activities for a set of inhibitors of VEGFR2 based on least squares support vector machines. In other report, Planesas et al. [26] proposed a three-step virtual screening protocol, which includes the conventional docking step, a pharmacophore postfilter step, and a similarity search postprocess and applied this protocol to the prediction of VEGFR2 inhibitors.

In the current work, we used the 3D-QSAR method comparative molecular field analysis (CoMFA) to explain the differences in activity between semaxanib and SU5205, and we studied the complexes that formed between these drugs and VEGFR2 using docking and MD simulations. We analyzed the dynamics and energetics of the interactions between the inhibitors and residues at the VEGFR2 active site.

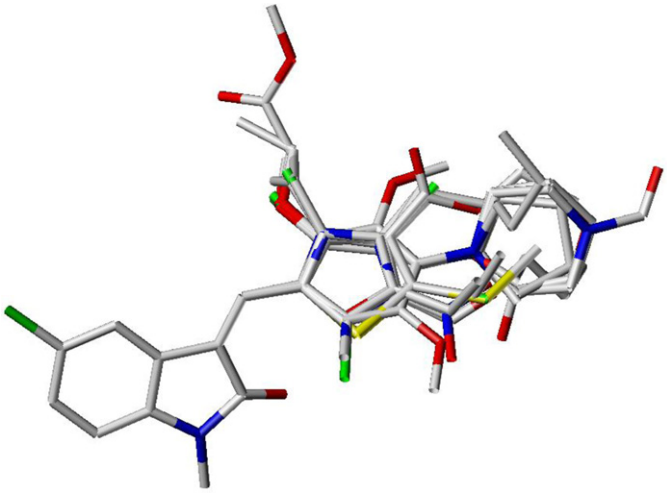

Fig. 2. Superposition used for CoMFA.

2. Methods and computational details

2.1. CoMFA

CoMFA [27] is a methodology of 3D-QSAR employing both interactive graphics and statistical techniques for correlating physico-chemical properties of molecules with their observed biological activities. For the molecules the steric and electrostatic interaction energies with a test probe atom are calculated at regularly spaced grid points surrounding the mutually aligned molecules. The contributions due to dispersion forces between molecules are described by Lennard–Jones-type potentials, and electrostatic properties are characterized by Coulomb-type potentials. Subsequent analysis of the calculated data by a partial least squares (PLS) cross-validation technique yields a set of coefficients which reflect the relative contribution of the physico-chemical elements of the molecules to differences in biological activities. 3D maps represented in an interactive graphics environment of the spatial volumes highly associated with biological activity yields an understanding of intermolecular associations. CoMFA can also predict the biological activity of new molecular species.

The primary structures and activities of 48 2-indolinone derivatives were taken from the patent of Tang et al. [28]. For the 3D-QSAR calculations, the compound set was randomly divided into a training set (40 compounds) and a test set (8 compounds). This subdivision was performed in such a way that both sets represent equally well the chemical and biological properties of the whole data set. Compounds SU4312, SU4793, SU4794, SU4798, SU4799, SU4932, SU4952, SU4967, SU4979, SU4981, SU4982, SU4983, SU4984, SU5204, SU5208, SU5214, SU5404, SU5405, SU5406, SU5407, SU5408, SU5418, SU5419, SU5421, SU5424,

Table 1
CoMFA analysis results.[a]

Model	NC	R^2	s	F	Q^2	s_{CV}	Fraction	
							Steric	Electrostatic
CoMFA-S	4	0.747	0.404	25.83	0.315	0.665	1	
CoMFA-E	1	0.070	0.744	2.88	−0.013	0.776		1
CoMFA-SE	5	0.848	0.318	37.92	0.517	0.578	0.544	0.456

[a] NC is the number of principal components from the PLS analysis; R^2 is the square of the correlation coefficient; s is the standard deviation of the regression; F is the Fisher ratio; and Q^2 and s_{CV} are the correlation coefficient and standard deviation, respectively, of the LOO cross-validation.

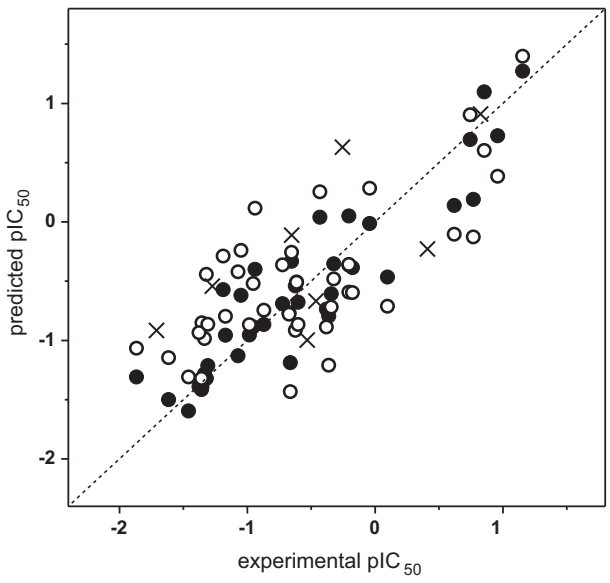

Fig. 3. Scatter plot of the experimental versus predicted activities for the CoMFA-SE model: (●) training set predictions; (○) LOO cross-validated predictions; and (×) test set predictions.

SU5427, SU5430, SU5431, SU5432, SU5453, SU5463, SU5464, SU5466, SU5468, SU5472, SU5473, SU5474, SU5480, semaxanib, and SU5205 were included in the training set, and compounds SU4313, SU4314, SU5401, SU5403, SU5425, SU5451, SU5455, and SU5477 were included in the test set. The VEGFR2 inhibitory activities of these compounds were recorded and transformed into pIC_{50} values. The IC_{50} value represents the micromolar concentration of each compound required to achieve 50% inhibition of VEGFR2. Sketching, optimization, and alignment of the molecules were achieved following the protocol described in reference [29] by considering the 2-indolinone scaffold as the fixed part of the molecules in optimization tasks.

QSAR modeling was performed using the SYBYL 7.3 software from Tripos [30]. First, the molecules were placed in a rectangular grid, and the interaction energies between a probe atom and all of the compounds were computed at the surrounding points using a volume-dependent lattice with 2.0 Å grid spacing. Then standard SYBYL parameters were used for PLS analysis. The number of components in the PLS models were optimized using a Q^2 value obtained from the leave-one-out (LOO) cross-validation procedure with the SAMPLS [31] sampling method. The CoMFA models were generated using steric and electrostatic probes with standard 30 kcal/mol cutoffs. The modeling capability (goodness of fit) was judged by the correlation coefficient squared, R^2. The prediction capability (goodness of prediction) was indicated by the Q^2 value and the prediction of the compounds from the test set.

2.2. Docking

Docking is a computational method which predicts the preferred orientation of one molecule to a second when bound to each other to form a stable complex. Knowledge of the preferred orientation may be used to predict the strength of association or binding affinity between two molecules using a scoring function. Docking has been widely used to suggest the binding modes of protein inhibitors. Most docking algorithms are able to generate a large number of possible structures, thus they also require a means to score each structure to identify those that are of the greatest interest. In general, the "docking problem" is concerned with the generation and evaluation of plausible structures of intermolecular complexes.

Docking was performed using Glide [32]. Glide docking uses a series of hierarchical filters to find the best possible ligand binding locations in a previously built receptor grid space. The filters include a systematic search approach, which samples the positional, conformational, and orientational space of the ligand before evaluating the energy interactions between the ligand and the protein [32]. The Glide program is contained in Maestro 9.0 software [33]. We used the standard-precision (SP) module of Glide. A grid box of 30 Å × 30 Å × 30 Å was first centered on the oxygen of the backbone carbonyl group of residue Glu917. Default docking parameters were used. The docking hierarchy begins with the systematic conformational expansion of the ligand followed by placement in the receptor site. Then minimization of the ligand in the field of the receptor is carried out using the OPLS-AA [34] force field with a distance-dependent dielectric of 2.0. Afterward, the lowest energy

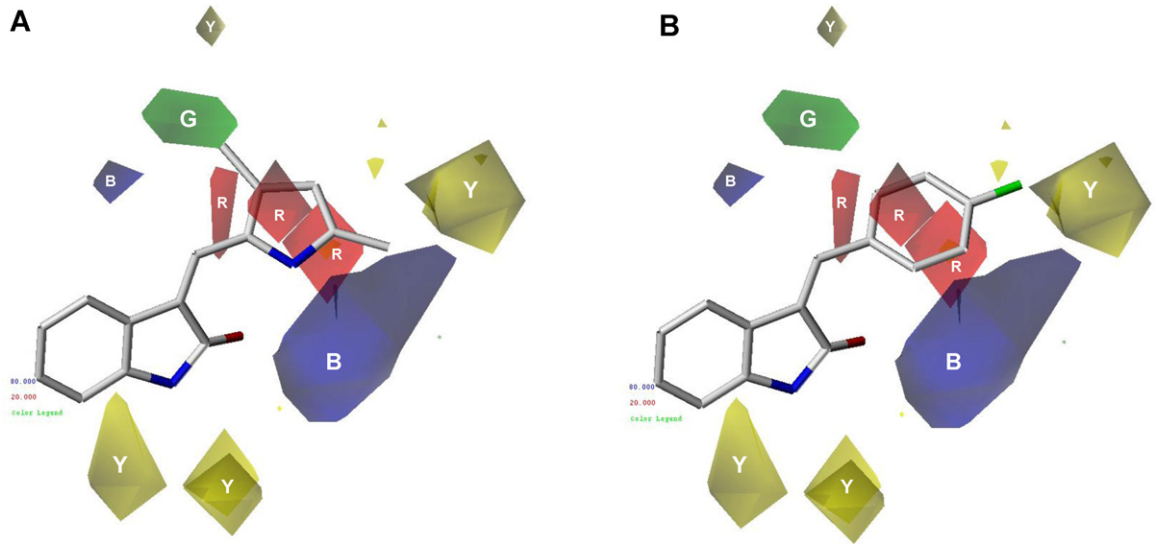

Fig. 4. CoMFA contour maps for 2-indolinone derivatives (CoMSIA-SE model). (A) Semaxanib is shown inside the fields. (B) SU5205 is shown inside the fields. Green isopleths indicate regions where bulky groups enhance the activity, and yellow isopleths indicate regions where bulky groups disfavor the activity. Blue isopleths indicate regions where an increase of positive charge enhances the activity, and red isopleths indicate regions where more negative charges are favorable for activity. (For interpretation of the references to color in this figure legend, the reader is referred to the web version of the article.)

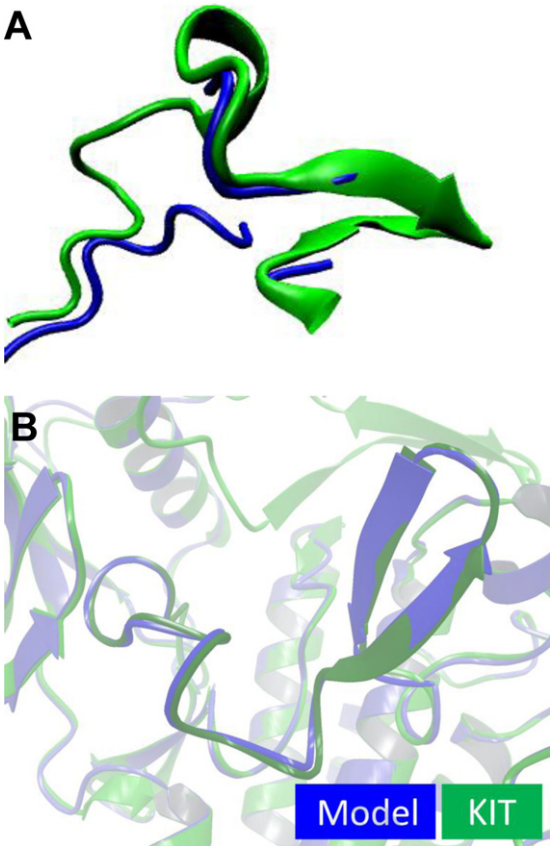

Fig. 5. Comparison between VEGFR2 and KIT. (A) Superimposition of the analogous loops of VEGFR2 (PDB: 3ewh) and KIT (PDB: 3g0e). (B) Superimposition of the analogous loops of VEGFR2 and KIT after homology modeling (VEGFR2 in blue and KIT in green). (For interpretation of the references to color in this figure legend, the reader is referred to the web version of the article.)

poses are subjected to a Monte Carlo (MC) procedure that samples the nearby torsional minima. The best pose for a given ligand is determined by the Emodel score, while different compounds are ranked using GlideScore, a modified version of the ChemScore function described by Eldridge et al. [35] that includes terms for buried polar groups and steric clashes.

The VEGFR2 structure was used as the template for the docking simulations. The protein coordinates were extracted from the X-ray crystal structure (accession code in Protein Data Bank (PDB): 3ewh). The structures of semaxanib and SU5205 were sketched with Maestro software [33]. The docking poses for each ligand were analyzed by examining their relative total energy score. The more energetically favorable conformation was selected as the best pose. The orientations obtained through the docking experiments were compared with the X-ray crystallographic structures of the complex containing KIT and sunitinib (SU11248) (accession code in PDB: 3g0e) [36].

2.3. MD simulations

The molecular dynamics of semaxanib and SU5205 inside the VEGFR2 active site were studied using the OPLS-AA force field in an explicit solvent with the single point charge (SPC) water model (OPLS-AA/SPC) [37] within the Desmond software [38,39] for the MD simulations. The initial coordinates for the MD calculations were taken from the docking experiments. The SPC water molecules were then added (the dimensions of each orthorhombic water box were approximately 84 Å × 79 Å × 65 Å, which ensured that the entire surface of each complex was covered by the solvent model), and the systems were neutralized by adding Cl^- counterions to balance the net charges of the systems. After the construction of the solvent environment, each complex system was composed of approximately 39,920 atoms. Before equilibration and long production MD simulations, the systems were minimized and pre-equilibrated using the default relaxation routine implemented in Desmond. For this, the program ran six steps composed of minimizations and short (12 and 24 ps) molecular dynamics simulations to relax the model system before performing the final long simulations. Then, a first 5 ns long equilibration MD simulation was performed on each complex system, and each system was followed for a 20 ns long production MD simulation. The OPLS-2005 [37] force field was used along with the MacroModel module [40] to provide and check the necessary force field parameters for the ligands. When MacroModel performs an energy calculation, the program checks the quality of each parameter in use. The use of low quality parameters, especially torsional ones, may result in inaccurate conformational energy differences and geometries. Bond, angle, torsional angle and improper angle checked parameters were listed as high- and medium-quality force field parameters for all ligand studied. During the MD simulations, the equations of motion were integrated with a 2 fs time step in the NVT ensemble. The SHAKE algorithm was applied to all hydrogen atoms; the van der Waals (VDW) cutoff was set to 9 Å. The temperature was maintained at 300 K, employing the Nosé–Hoover thermostat method with a relaxation time of 1 ps. Long-range electrostatic forces were taken into account by means of the particle-mesh Ewald (PME) approach. Data were collected every 1 ps during the MD runs. Visualization of protein–ligand complexes and MD trajectory analysis were carried out with the VMD software package [41].

Table 2
The relevant stable geometrical parameters between the atoms of the inhibitors and the atoms of VEGFR2 during the MD simulations.

Compound	D1 (Å)[a]	D2 (Å)[b]	φ (°)[c]
Semaxanib	2.979 ± 0.176	2.871 ± 0.140	−5.184 ± 8.714
SU5205	3.107 ± 0.224	2.791 ± 0.129	−20.703 ± 16.589

[a] Distance between the nitrogen from the oxindole group and the oxygen from the backbone of Glu917.
[b] distance between the oxygen from the oxindole group and the nitrogen from the backbone of Cys919.
[c] Dihedral angle (a–d as defined in Fig. 1) between oxindole group and *R* substituent.

3. Results and discussion

3.1. CoMFA results

Fig. 2 shows the aligned molecules within the grid box used to generate the CoMFA columns. First, we developed the CoMFA models by including one field. Then we combined these fields and analyzed the statistical quality of the hybrid models by considering the Q^2 values [10]. The results are presented in Table 1. The CoMFA models describing VEGFR2 inhibition that used only the steric field or the electrostatic field (models CoMFA-S and CoMFA-E) were statistically unacceptable ($Q^2 < 0.5$). However, when both fields were considered (model CoMFA-SE), a CoMFA model with a higher statistical significance ($Q^2 = 0.517$) was obtained. These results reveal that both the steric and electrostatic features of the studied molecules have a major influence on the VEGFR2 inhibitory activity. The model indicated a steric contribution of 54.4% and an electrostatic contribution of 45.6%. The CoMFA-SE model also adequately predicted the inhibitory activities of the test set compounds. The correlations between the calculated and experimental values of pIC_{50} (from training, LOO cross-validation and test set) are shown in Fig. 3.

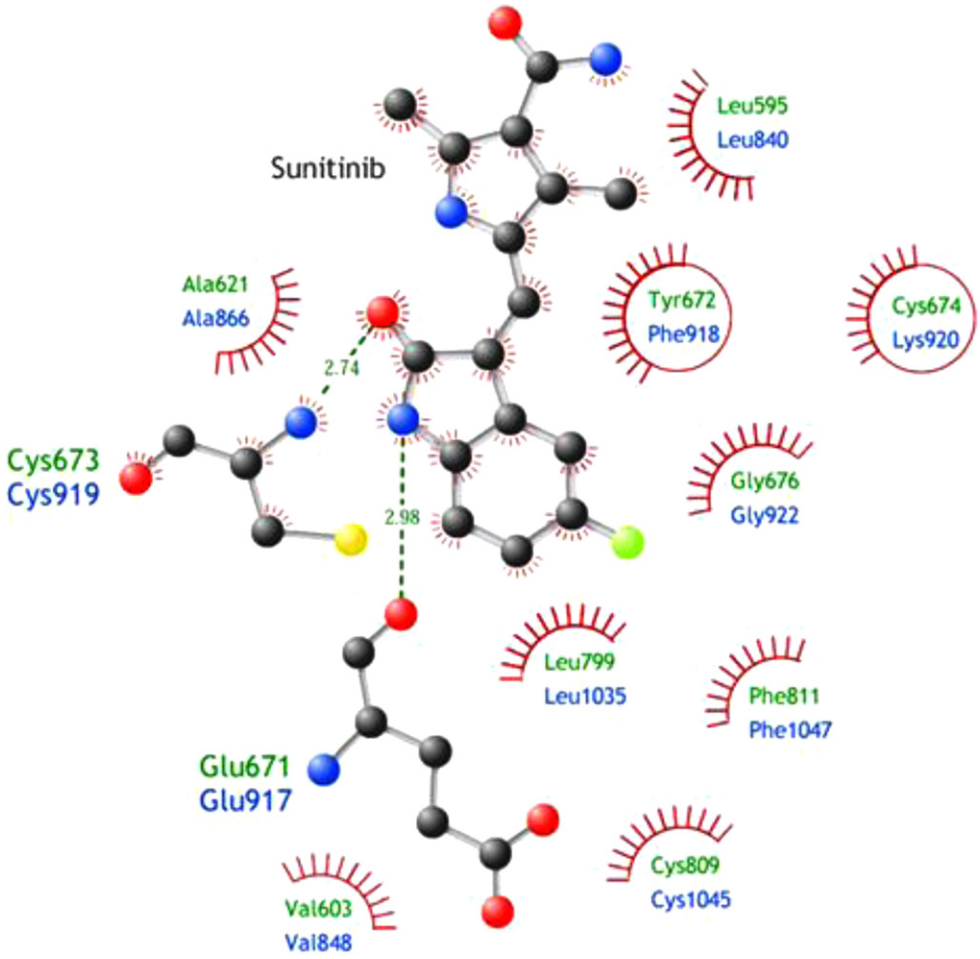

Fig. 6. Residues comprising the active sites of VEGFR2 and KIT in complex with the oxindole scaffold of sunitinib.

The contour plots of the CoMFA steric and electrostatic fields are presented in Fig. 4. To aid in visualization, semaxanib and SU5205 are displayed in the maps. In general, the colored isopleths in the map surround all lattice points where the QSAR strongly associated changes in the compounds' field values with changes in biological potency. Green and yellow isopleths indicate regions where bulky groups favored and disfavored the activity, respectively. A green contour near the methyl group at position 4 of the (pyrrol-5-yl)methylene substituent in semaxanib indicates that the presence of a bulky group has a positive effect on the compound's VEGFR2 inhibitory activity. SU5205 lacks a group with these characteristics. On the other hand, yellow isopleths near the F group of the 4-fluorobenzylidene substituent in SU5205 indicate that bulky groups have a negative effect on VEGFR2 inhibitory activity. Semaxanib does not contain a bulky group in this zone. The other yellow isopleths at position 1 of the 2-indolinone scaffold indicate that bulky groups at this position have a negative impact on the inhibitory activity; indeed, compounds SU4952 and SU4982 have a methyl group at this position and have poor inhibitory activities. The blue and red isopleths indicate regions where positive and negative charges, respectively, favored the activity (Fig. 4). A blue contour near position 1 of the (pyrrol-5-yl)methylene substituent in semaxanib indicates that a positively charged group contributes to its high inhibitory activity. Red contours in the surroundings of the (pyrrol-5-yl)methylene and 4-fluorobenzylidene substituents indicate that R groups with a negative density are preferred in this zone.

It was further found that increasing the steric bulk of the substituent next to the methylene (position 4 of the (pyrrol-5-yl)methylene and position 2 of the 4-fluorobenzylidene) or diminishing the steric bulk of the substituent at position 4 of the fluorobenzylidene correlates with a stronger inhibition of VEGFR2. These features related to the structure–activity relationship encountered by CoMFA are certainly true for semaxanib and SU5205. The structural information contained in the set of 2-indolinone derivatives that is relevant for VEGFR2 inhibition indicates that 4-fluorobenzylidene is an inappropriate substituent and that some modifications could improve the activity. For instance, the replacement of 4-fluorobenzylidene by 2-fluorobenzylidene or 5-fluoro-2-methylbenzylidene should lead to ^{18}F-labeled radiotracers with a higher inhibitory activity.

3.2. Docking results

The X-ray structures of VEGFR2 in the PDB do not contain the loop after the DFG motif, which includes residues from 1048 to 1068. The X-ray structure denoted by 3ewh in the PDB contains some residues of this loop; their positions are similar to the positions of the analogue residues in the tyrosine-protein kinase KIT (accession code in PDB: 3g0e) (Fig. 5A). In this sense, a new model containing this loop was built using homology modeling and the structure of KIT as a template. The resulting loop structure is shown in Fig. 5B.

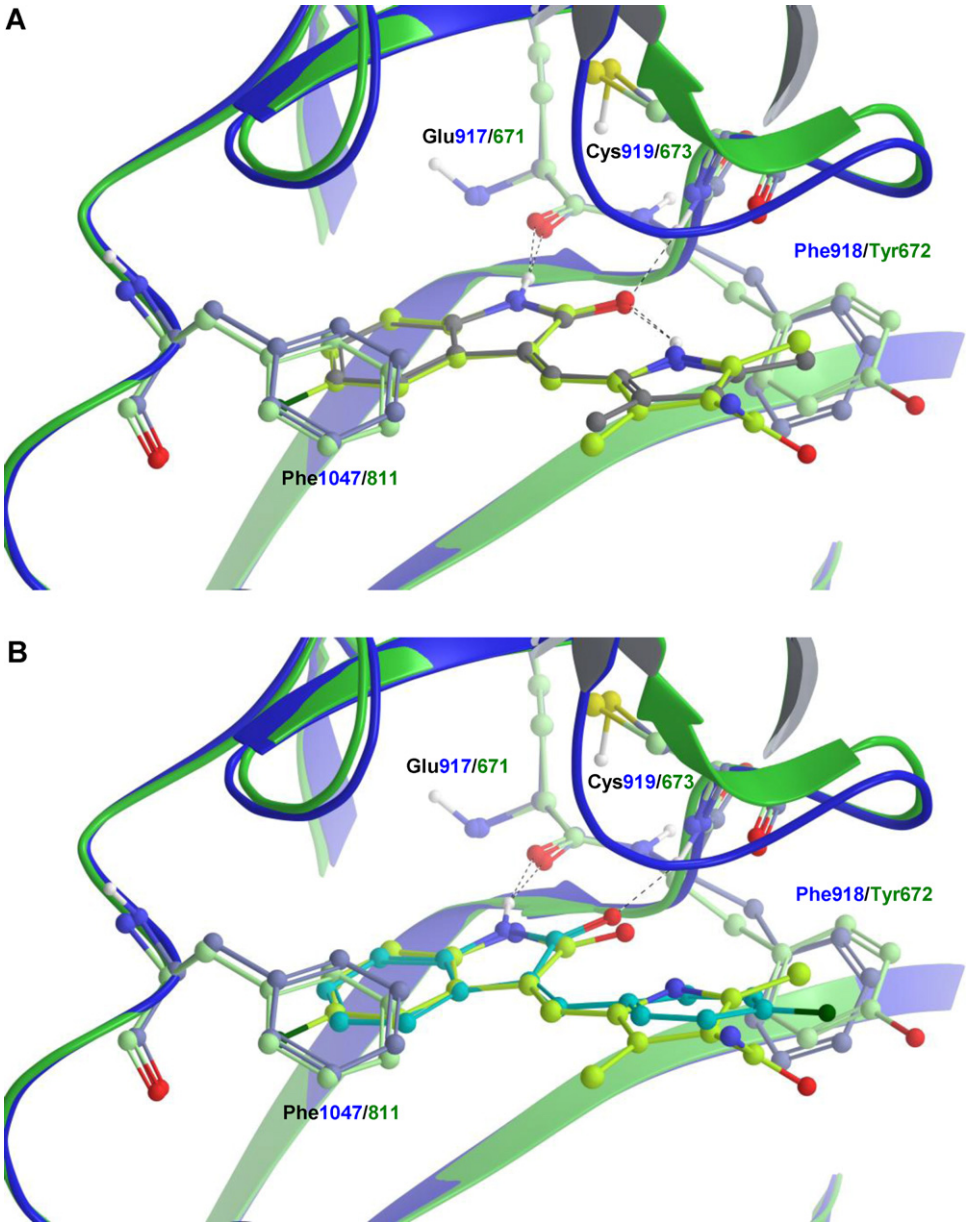

Fig. 7. (A) VEGFR2/semaxanib and (B) VEGFR2/SU5205 complexes proposed by docking (VEGFR2 in blue, semaxanib in gray, and SU5205 in cyan). The sunitinib/KIT complex is also represented for comparison of the orientations of the inhibitors (KIT in green and sunitinib in light green). Nonpolar hydrogens are omitted for clarity. (For interpretation of the references to color in this figure legend, the reader is referred to the web version of the article.)

The X-ray structure of KIT kinase denoted by 3g0e in the PDB contains the inhibitor sunitinib in its active site. Sunitinib is a kinase inhibitor that contains an oxindole scaffold like that of semaxanib. The active sites of KIT and VEGFR2 are quite similar (Fig. 6); Tyr672 and Cys674 in KIT are replaced by Phe918 and Lys920 in VEGFR2, respectively. Therefore, we expected that the oxindole scaffold should be oriented inside VEGFR2's active site in a similar manner with respect to the orientation in KIT. Thus, the orientations obtained from the docking experiments on VEGFR2's active site were compared with the X-ray crystallographic structure of the complex containing KIT and the oxindole scaffold of sunitinib. As can be observed in Fig. 7, the docked structures showed the same orientation of the inhibitor in VEGFR2 with respect to the known orientation of the oxindole scaffold in KIT. The values of the root-mean square deviations (RMSDs) for the docked structures with respect to the X-ray crystallographic structure of the inhibitor (considering only the oxindole scaffold in KIT) were 0.069 and 0.290 Å.

Both inhibitors (semaxanib and SU5205) adopted the same binding mode; this is not surprising because both compounds contain the same scaffold and similar substituents. The following are true for both compounds:

a) The oxindole group is surrounded by Phe1047, Val848, Ala866, Lys868, Val899, Glu917, Phe918, Cys919, and Leu840, and it forms hydrogen bond (HB) interactions between the NH of the oxindole and the backbone carbonyl group of Glu917 and between the carbonyl of the oxindole and the backbone NH of Cys919.
b) Group R (Fig. 1) is at the entrance of the pocket and is surrounded by Leu840, Phe1047, Phe918, Gly922, and Asn923.

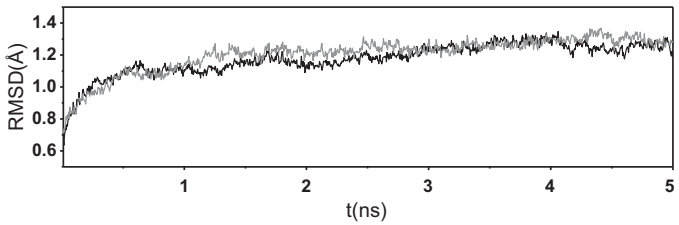

Fig. 8. Time dependence of the RMSD for the backbone from the starting structures during the equilibration process. RMSDs for systems containing semaxanib and SU5205 are represented in black and gray, respectively.

R groups (3,5-dimethyl-1*H*-pyrrol-2-yl and 4-fluorophenyl) determine the differences between both inhibitors. Therefore, the interactions with the VEGFR2 residues involving these groups seem to be responsible of the differences between the inhibitory activities for semaxanib and SU5205.

3.3. MD results

Both compounds showed the same orientation, but 3,5-dimethyl-1*H*-pyrrol-2-yl and 4-fluorophenyl groups interact with several residues at the entrance of the VEGFR2 active site. Despite the small differences in the substituents, semaxanib and SU5205 have considerable differences in their activities against VEGFR2 (Fig. 1). The use of explicit-water MD calculations allows for the analysis of the movement of the systems and the effect of the solvent in the formation of the complexes. The aim is to explain the differences in the activities for these compounds.

The RMSDs of the positions for all side chain atoms from their initial configuration as a function of simulation time (only the first 5 ns of equilibration MD are represented) for the investigated systems are shown in Fig. 8. The dependences of the RMSD values were tested to check whether convergence of the calculations was obtained and whether the equilibrated MD trajectory was stable. The RMSD values remain within 1.1 Å for both systems; this demonstrates the conformational stabilities of the protein structures.

Throughout the 20 ns long production MD simulations, the studied compounds were in the expected orientations. In both simulations, the NH of the oxindole group established an HB interaction with the backbone carbonyl group of Glu917, and the carbonyl group of the oxindole scaffold established an HB interaction with the backbone NH of Cys919. Table 2 shows that these interactions were stable during all simulations. The distance between the nitrogen from the oxindole group and the oxygen from the backbone of Glu917 (D1 in Table 2) was approximately 3.0 ± 0.2 Å, while the distance between the oxygen from the oxindole ring and the nitrogen from the backbone of Cys919 (D2 in Table 2) was approximately 2.8 ± 0.1 Å for both complexes.

The 3,5-dimethyl-1*H*-pyrrol-2-yl and 4-fluorophenyl groups did not form HBs with the residues at the entrance of the VEGFR2 binding site. The torsional angles φ between the oxindole group and the R substituent (torsional angle a–d as represented in Fig. 1) were measured based on the 20-ns dynamics and are shown in Table 2. This angle was -5.184 ± 8.714 for semaxanib, which indicates that the inhibitor is almost planar inside the VEGFR2 active site. This planarity is due to the presence of an intramolecular HB formed between the oxygen of the oxindole and the NH of the 3,5-dimethyl-1*H*-pyrrol-2-yl group. On the other hand, the angle φ was -20.703 ± 16.589 for SU5205. Although SU5205 is characterized by a conjugated aromaticity, the φ value indicates that the inhibitor is not completely planar inside the VEGFR2 active site; in this sense, it has a lower aromaticity. The lower aromaticity of SU5205 should have implications for the interactions between the inhibitor and the hydrophobic residues. Aromaticity has been identified in quantitative structure–activity relationship (QSAR) studies as a descriptor of the differences in activity between inhibitors [42–45]. In general, the aromaticity has been described as the number of aromatic atoms, aromatic rings, or aromatic bonds in QSAR studies; however, the effect of the planarity on aromaticity has not usually been taken into account in these studies.

The interaction energies between the residues in the active site and the inhibitors within the complex structures were examined using the ASET script included in the MacroModel module [40] from the Schrödinger Suite of computational programs. These calculations were applied to ten snapshots randomly selected from the MD trajectories. Fig. 9 shows the total free energy contributions with respect to residue number where total free energy includes the VDW as well as the electrostatic and solvation free energies. In general, this analysis did not show differences because all residues showed similar contributions in both complexes. The residue Lys868 has a high positive energy value for both complexes, indicating that this residue is unfavorable for binding of semaxanib and SU5205. The positive charge on the side chain of Lys868 is close to position 6 of the oxindole group, which is the more hydrophobic part of the inhibitor. The Glu917 and Cys919 residues are more favorable for binding and are involved in the hydrogen bonding.

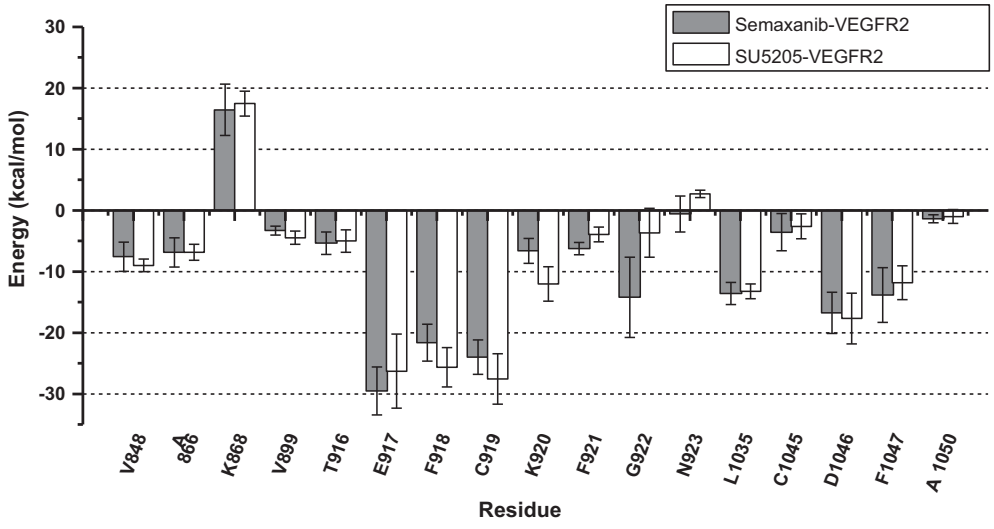

Fig. 9. Free energy decomposition plot for interaction between semaxanib and SU5205 and amino acids in the active site of VEGFR2.

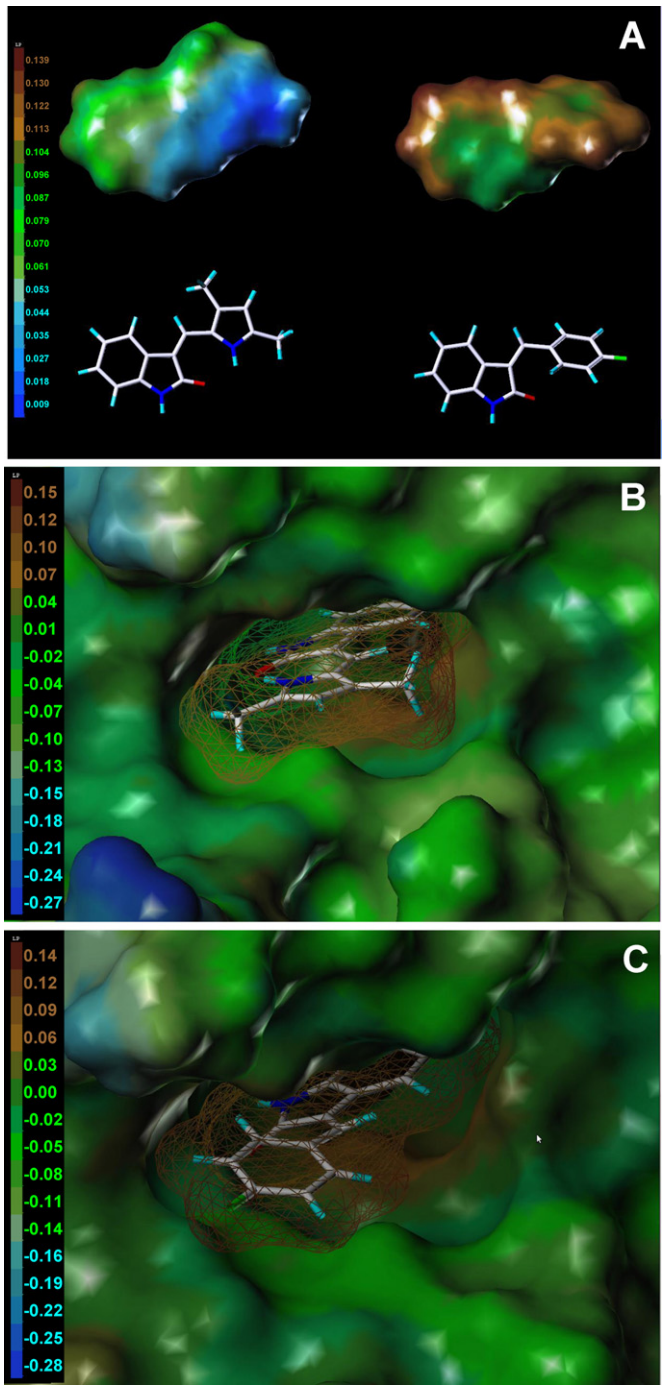

Fig. 10. Lipophilic potential (LP) for (A) semaxanib and SU5205; (B) semaxanib inside the VEGFR2 active site; (C) SU5205 inside the VEGFR2 active site. The Fast Connolly surface generated by MOLCAD is colored by the LP, which ranges from brown (highest lipophilic area) to blue (highest hydrophilic area).

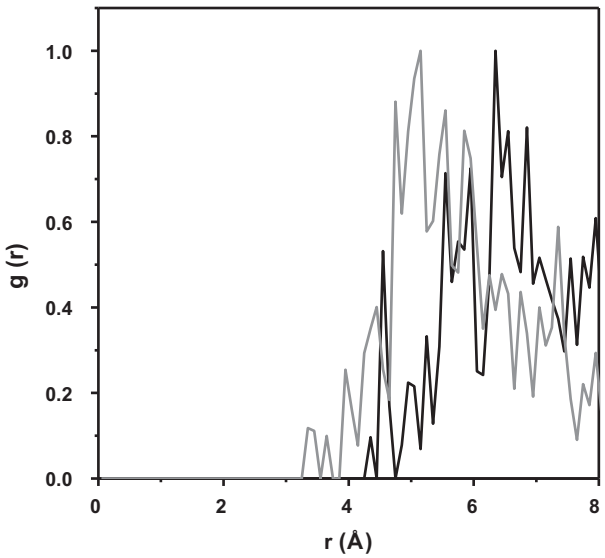

Fig. 11. Water radial distribution functions calculated from 20-ns MD simulations. Water molecules at a distance ≤7 Å from the carbon atom denoted as b in Fig. 1 for the semaxanib–VEGFR2 complex (black) and for the SU5205–VEGFR2 complex (gray).

Finally Phe918 is only implicated in hydrophobic interactions with the R groups of both inhibitors.

The surfaces generated by MOLCAD [46] combining the Fast Connolly surfaces (steric properties) and the molecular lipophilicity potential (MLP) maps (lipophilic properties) allow for the analysis of the non-bonded interactions between the inhibitor and the receptor. Color-coded visualization of the MLPs of semaxanib and SU5205 indicates that SU5205 is more hydrophobic (Fig. 10A). In Fig. 10B and C, the Fast Connolly surfaces are represented for the semaxanib–VEGFR2 and SU5205–VEGFR2 complexes, respectively. The 3,5-dimethyl-1*H*-pyrrol-2-yl and 4-fluorophenyl groups have more hydrophobic surfaces with respect to the surface of the active site at the entrance of the pocket. This part of the pocket has some hydrophobic residues, such as Leu840, Phe1047, Phe918, and Gly922. The 3,5-dimethyl-1*H*-pyrrol-2-yl group is able to cover all of the entrance of the active site (Fig. 10B) and interacts with these residues. However, the 4-fluorophenyl group occupies only a small part of the entrance of the active site (Fig. 10C), which could lead to the presence of more water molecules inside the active site.

We further explored the water environment around the inhibitors in the active site of VEGFR2. We calculated the radial distribution function (RDF) between the carbon atom denoted as b in Fig. 1 and the water molecules at a distance ≤7 Å from this selected atom for both complexes. This carbon atom was selected because it is in an approximately central position in the active site for both complexes. The selection of water molecules at a distance ≤7 Å guarantees that only solvent inside the active site is considered. Fig. 11 shows the RDFs derived from 20-ns MD simulations. The plots show that the probability of finding a water molecule inside the VEGFR2 active site is higher at distances below 5.5 Å from the central position of the active site for the SU5205–VEGFR2 complex. In this sense, the analysis of the dynamics reveals that the hydrophobic residues at the entrance of the active site and the hydrophobic 4-fluorophenyl group are more exposed to the solvent. Instead, the 3,5-dimethyl-1*H*-pyrrol-2-yl group can establish interactions with the above-mentioned residues and restrict the entry of water molecules inside the active site.

We evaluated the association of the ligands with the receptor using Multi-Ligand Biomolecular Association with Energetics (Embrace) from the MacroModel module [40] in the interaction mode. With Embrace, ligands can be minimized within the receptor. As a result, Embrace gives an estimation of the binding affinity considering the VDW and the electrostatic terms. The averaged energy values obtained from Embrace calculations applied to ten snapshots from 20-ns MD simulations are reported in Table 3. The total energy values E_{Tot} showed that interaction is more favorable for the semaxanib–VEGFR2 complex. If we examine the contributions to binding, there is an increase in the VDW contribution (E_{VDW}) as the interaction becomes more favorable. This appears to explain the higher affinity of semaxanib because, while the electrostatic energy term E_{Elect} remains relatively constant across both

Table 3
The average energy contributions to the binding energy between VEGFR2 and the inhibitors obtained from snapshots of MD simulations using Embrace calculations.[a]

Complex	E_{Tot} (kcal/mol)	E_{VDW} (kcal/mol)	E_{Elect} (kcal/mol)
Semaxanib–VEGFR2	−52.132 ± 1.664	−36.278 ± 1.044	−15.854 ± 1.651
SU5205–VEGFR2	−48.905 ± 1.624	−32.585 ± 1.060	−16.320 ± 1.704

[a] E_{Tot}, total energy; E_{VDW}, VDW energy term; E_{Elect}, electrostatic energy term.

Table 4
Calculated binding free energies for VEGFR2–ligand complexes using MM-GBSA for the snapshots of MD simulations.

Complex	$\Delta E_{internal}$ (kcal/mol)	ΔE_{Elect} (kcal/mol)	ΔE_{VDW} (kcal/mol)	ΔG_{solvGB} (kcal/mol)	ΔG_{solvSA} (kcal/mol)	$T\Delta S$ (kcal/mol)	ΔG_{bind} (kcal/mol)
Semaxanib–VEGFR2	0.707 ± 0.369	−14.640 ± 1.271	−40.260 ± 1.022	14.521 ± 1.003	1.940 ± 0.528	−13.491 ± 0.550	−24.241 ± 2.267
SU5205–VEGFR2	0.863 ± 0.731	−13.901 ± 1.025	−35.417 ± 1.163	13.146 ± 1.408	−0.470 ± 0.343	−14.934 ± 0.769	−20.845 ± 1.435
Difference (absolute values)	0.156	0.739	4.843	1.375	2.41	1.443	3.396

complexes, semaxanib has added nonpolar packing in the active site. The better binding of semaxanib gains over 3.69 kcal/mol of VDW energy compared with SU5205.

We also estimated the binding-free energy (ΔG_{bind}) of each ligand using Prime molecular mechanics-generalized Born surface area (MM-GBSA) method [47,48]. The calculations were performed on each complex system using ten snapshots from 20-ns MD simulations. The following equation was used:

$$\Delta G_{bind} = \Delta E_{MM} + \Delta G_{solv} - T\Delta S \quad (1)$$

where ΔE_{MM} is the change of the gas phase MM energy upon binding, and includes $\Delta E_{internal}$ (bond, angle, and dihedral energies), ΔE_{Elect} (electrostatic), and ΔE_{VDW} (van der Waals) energies. ΔG_{solv} is the change of the solvation free energy upon binding, and includes the electrostatic solvation free energy ΔG_{solvGB} (polar contribution calculated using generalized Born model), and the nonelectrostatic solvation component ΔG_{solvSA} (nonpolar contribution estimated by solvent accessible surface area). Finally, $T\Delta S$ is the change of the conformational entropy upon binding; this term was calculated using normal-mode analysis RRHO contained in MacroModel module [40]. The averaged energy values obtained from MM-GBSA calculations are reported in Table 4. The ΔG_{bind} value also showed that interaction is more favorable for the semaxanib–VEGFR2 complex (the difference in the calculated ΔG_{bind} value between both inhibitors was 3.396 kcal/mol). According to the energy components of the binding free energies (Table 4), the major favorable contributors to ligand binding are VDW and electrostatic terms, whereas polar solvation (ΔG_{solvGB}) and entropy terms oppose binding. Nonpolar solvation terms (ΔG_{solvSA}) contribute slightly unfavorably for the complex with semaxanib and slightly favorably for the complex with SU5205. If we examine the contributions to each binding energy, the most important term which dictates the difference in the binding affinity is ΔE_{VDW}. The better binding of semaxanib gains over 4.843 kcal/mol of ΔE_{VDW} value compared with SU5205, which is the key factor for the more favorable ΔG_{bind} value for semaxanib. This is in agreement with the results previously obtained using Embrace calculations.

As discussed above, our MD simulations suggest that the 3,5-dimethyl-1*H*-pyrrol-2-yl substituent facilitates better positioning of semaxanib in the active site and thus better VDW interactions with the protein. The presence of the 4-fluorophenyl group leads to a more hydrophobic oxindole derivative with lower aromaticity when it interacts with VEGFR2. In addition, when SU5205 forms the inhibitor–enzyme complex, more water molecules enter the VEGFR2 active site. Binding energy calculations reflect this event: VDW terms have the main contribution to the difference of the binding energy between both inhibitors because 3,5-dimethyl-1 *H*-pyrrol-2-yl substituent in semaxanib has better VDW interactions with protein residues than 4-fluorophenyl group in SU5205.

4. Conclusions

We studied semaxanib and SU5205 and their complexes with VEGFR2 to determine the reasons for their different inhibitory activities toward this enzyme. We used several methods that together explain the difference:

- We obtained a CoMFA model that accurately defined the molecular basis for the inhibition of VEGFR2 by 2-indolinone derivatives. The comparison of the contour maps obtained from the CoMFA model with the structures of semaxanib and SU5205 allowed for identification of the structural features responsible for the difference in activity between these compounds. The CoMFA model can orient the design of new 2-indolinone derivatives containing F atoms that can represent putative radiotracers.
- Molecular docking was used to predict the orientation of semaxanib and SU5205 within the VEGFR2 binding site. Both inhibitors were oriented in a similar manner compared with the known orientation of the oxindole scaffold in KIT.
- We also studied the dynamics of the complexes, and we found that both inhibitors established similar stable interactions inside the VEGFR2 active site. The analysis of the energetic contribution of each amino acid to the binding of the inhibitor was also similar.
- From the analysis of the molecular lipophilicity potential (MLP) maps for semaxanib and SU5205, we found that SU5205 is a more hydrophobic molecule.
- The analysis of the water environment inside the active site during the molecular dynamics experiments showed that more water molecules enter the VEGFR2 active site when the complex with the more hydrophobic inhibitor SU5205 is formed. This should lead to the greater instability of this complex.
- The analysis of the energetic binding components using Embrace and MM-GBSA methods reveals that while the VDW energy drives binding of the inhibitors, electrostatic energy alone does not completely explain the affinity differential.

Finally, we suggest that the differences in activity between semaxanib and SU5205 can be attributed to different the hydrophobicities of these molecules, and the VDW interactions with protein residues toghether with the effect of the solvent when their complexes with VEGFR2 are formed.

Acknowledgements

J.H.A.M. acknowledges the financial support from the project FONDECYT No. 11100177. J.C. and A.V.J. are grateful to "Becas Universidad de Talca" for financial support through a doctoral fellowship.

References

[1] D.B. Mendel, R.E. Schreck, D.C. West, G. Li, L.M. Strawn, S.S. Tanciongco, et al., The angiogenesis inhibitor SU5416 has long-lasting effects on vascular endothelial growth factor receptor phosphorylation and function, Clin. Cancer Res. 6 (2000) 4848–4858.

[2] D. Hanahan, R.A. Weinberg, The hallmarks of cancer, Cell 100 (2000) 57–70.

[3] S. Yearn, L. Kyung-Han, Targeted in vivo imaging of angiogenesis: present status and perspectives, Curr. Pharm. Des. 13 (2007) 17–31.

[4] T. Kniess, R. Bergmann, M. Kuchar, J. Steinbach, F. Wuest, Synthesis and radiopharmacological investigation of 3-[4′-[18F]fluorobenzylidene]indolin-2-one as possible tyrosine kinase inhibitor, Bioorg. Med. Chem. 17 (2009) 7732–7742.

[5] J.H. Alzate-Morales, J. Caballero, A. Vergara-Jaque, F.D. González-Nilo, Insights into the structural basis of N2 and O6 substituted guanine derivatives as cyclin-dependent kinase 2 (CDK2) inhibitors: prediction of the binding modes and potency of the inhibitors by docking and ONIOM calculations, J. Chem. Inf. Model. 49 (2009) 886–899.

[6] C.A. Larsen, W.H. Bisson, R.H. Dashwood, Tea catechins inhibit hepatocyte growth factor receptor (MET kinase) activity in human colon cancer cells: kinetic and molecular docking studies, J. Med. Chem. 52 (2009) 6543–6545.

[7] J. Caballero, M. Quiliano, J.H. Alzate-Morales, M. Zimic, E. Deharo, Docking and quantitative structure–activity relationship studies for 3-fluoro-4-(pyrrolo[2,1-f][1,2,4]triazin-4-yloxy)aniline, 3-fluoro-4-(1*H*-pyrrolo[2,3-b]pyridin-4-yloxy)aniline, and 4-(4-amino-2-fluorophenoxy)-2-pyridinylamine derivatives as c-Met kinase inhibitors, J. Comput.-Aided Mol. Des. 25 (2011) 349–369.

[8] M. Fernandez, A. Tundidor-Camba, J. Caballero, Modeling of cyclin-dependent kinase inhibition by 1H-pyrazolo[3,4-d]pyrimidine derivatives using artificial neural network ensembles, J. Chem. Inf. Model. 45 (2005) 1884–1895.

[9] M. González, J. Caballero, A. Helguera, M. Garriga, G. González, M. Fernández, 2D autocorrelation modelling of the inhibitory activity of cytokinin-derived cyclin-dependent kinase inhibitors, Bull. Math. Biol. 68 (2006) 735–751.

[10] J. Caballero, M. Fernández, M. Saavedra, F.D. González-Nilo, 2D autocorrelation, CoMFA, and CoMSIA modeling of protein tyrosine kinases' inhibition by substituted pyrido[2,3-d]pyrimidine derivatives, Bioorg. Med. Chem. 16 (2008) 810–821.

[11] J. Caballero, M. Fernández, F.D. González-Nilo, Structural requirements of pyrido[2,3-d]pyrimidin-7-one as CDK4/D inhibitors: 2D autocorrelation, CoMFA and CoMSIA analyses, Bioorg. Med. Chem. 16 (2008) 6103–6115.

[12] C. Gueto, J.L. Ruiz, J.E. Torres, J. Méndez, R. Vivas-Reyes, Three-dimensional quantitative structure–activity relationship studies on novel series of benzotriazine based compounds acting as Src inhibitors using CoMFA and CoMSIA, Bioorg. Med. Chem. 16 (2008) 2439–2447.

[13] J. Alzate-Morales, J. Caballero, Computational study of the interactions between guanine derivatives and cyclin-dependent kinase 2 (CDK2) by CoMFA and QM/MM, J. Chem. Inf. Model. 50 (2010) 110–122.

[14] D. Muthas, Y.A. Sabnis, M. Lundborg, A. Karlén, Is it possible to increase hit rates in structure-based virtual screening by pharmacophore filtering? An investigation of the advantages and pitfalls of post-filtering, J. Mol. Graph. Model. 26 (2008) 1237–1251.

[15] H.-Z. Xie, L.-L. Li, J.-X. Ren, J. Zou, L. Yang, Y.-Q. Wei, et al., Pharmacophore modeling study based on known spleen tyrosine kinase inhibitors together with virtual screening for identifying novel inhibitors, Bioorg. Med. Chem. Lett. 19 (2009) 1944–1949.

[16] M. Uno, H.S. Ban, W. Nabeyama, H. Nakamura, de novo Design and synthesis of N-benzylanilines as new candidates for VEGFR tyrosine kinase inhibitors, Org. Biomol. Chem. 6 (2008) 979–981.

[17] M. Vieth, J. Erickson, J. Wang, Y. Webster, M. Mader, R. Higgs, et al., Kinase inhibitor data modeling and de novo inhibitor design with fragment approaches, J. Med. Chem. 52 (2009) 6456–6466.

[18] J.H. Alzate-Morales, R. Contreras, A. Soriano, I. Tuñon, E. Silla, A computational study of the protein–ligand interactions in CDK2 inhibitors: using quantum mechanics/molecular mechanics interaction energy as a predictor of the biological activity, Biophys. J. 92 (2007) 430–439.

[19] M.P. Gleeson, D. Gleeson, QM/MM as a tool in fragment based drug discovery. A cross-docking, rescoring study of kinase inhibitors, J. Chem. Inf. Model. 49 (2009) 1437–1448.

[20] J.H. Alzate-Morales, J. Caballero, F.D. Gonzalez-Nilo, R. Contreras, A computational ONIOM model for the description of the H-bond interactions between NU2058 analogues and CDK2 active site, Chem. Phys. Lett. 479 (2009) 149–155.

[21] O. Villacañas, J.J. Pérez, J. Rubio-Martínez, Structural analysis of the inhibition of Cdk4 and Cdk6 by p16INK4a through molecular dynamics simulations, J. Biomol. Struct. Dyn. 20 (2002) 347–358.

[22] J. Du, B. Lei, J. Qin, H. Liu, X. Yao, Molecular modeling studies of vascular endothelial growth factor receptor tyrosine kinase inhibitors using QSAR and docking, J. Mol. Graph. Model. 27 (2009) 642–654.

[23] F.A. Pasha, M. Muddassar, M.M. Neaz, S.J. Cho, Pharmacophore and docking-based combined in-silico study of KDR inhibitors, J. Mol. Graph. Model. 28 (2009) 54–61.

[24] H. Zeng, H. Zhang, Combined 3D-QSAR modeling and molecular docking study on 1,4-dihydroindeno[1,2-c]pyrazoles as VEGFR-2 kinase inhibitors, J. Mol. Graph. Model. 29 (2010) 54–71.

[25] J. Li, J. Qin, H. Liu, X. Yao, M. Liu, Z. Hu, In silico prediction of inhibition activity of pyrazine–pyridine biheteroaryls as VEGFR-2 inhibitors based on least squares support vector machines, QSAR Comb. Sci. 27 (2008) 157–164.

[26] J.M. Planesas, R.M. Claramunt, J. Teixidó, J.I. Borrell, V.I. Pérez-Nueno, Improving VEGFR-2 docking-based screening by pharmacophore postfiltering and similarity search postprocessing, J. Chem. Inf. Model. 51 (2011) 777–787.

[27] R.D. Cramer, D.E. Patterson, J.D. Bunce, Comparative molecular field analysis (CoMFA). 1. Effect of shape on binding of steroids to carrier proteins, J. Am. Chem. Soc. 110 (1988) 5959–5967.

[28] P.C. Tang, L. Sun, G. McMahon, 3-(2′-Alkoxybenzylidenyl)-2-indolinone and analogues thereof for the treatment of disease, U.S. Patent 5,883,116, 1999.

[29] J. Caballero, M. Fernández, D. Coll, Quantitative structure–activity relationship of organosulphur compounds as soybean 15-lipoxygenase inhibitors using CoMFA and CoMSIA, Chem. Biol. Drug Des. 76 (2010) 511–517.

[30] SYBYL, Version 7.3, Tripos Inc., 1699 South Hanley Rd., St. Louis, MO 63144, USA, 2006.

[31] B.L. Bush, R.B. Nachbar, Sample-distance partial least squares: PLS optimized for many variables, with application to CoMFA, J. Comput.-Aided Mol. Des. 7 (1993) 587–619.

[32] R.A. Friesner, J.L. Banks, R.B. Murphy, T.A. Halgren, J.J. Klicic, D.T. Mainz, et al., Glide: a new approach for rapid, accurate docking and scoring. 1. Method and assessment of docking accuracy, J. Med. Chem. 47 (2004) 1739–1749.

[33] Maestro, Version 9.0, Schrödinger, LLC, New York, NY, 2007.

[34] W.L. Jorgensen, D.S. Maxwell, J. Tirado-Rives, Development and testing of the OPLS all-atom force field on conformational energetics and properties of organic liquids, J. Am. Chem. Soc. 118 (1996) 11225–11236.

[35] M.D. Eldridge, C.W. Murray, T.R. Auton, G.V. Paolini, R.P. Mee, Empirical scoring functions: I. The development of a fast empirical scoring function to estimate the binding affinity of ligands in receptor complexes, J. Comput.-Aided Mol. Des. 11 (1997) 425–445.

[36] K.S. Gajiwala, J.C. Wu, J. Christensen, G.D. Deshmukh, W. Diehl, J.P. DiNitto, et al., KIT kinase mutants show unique mechanisms of drug resistance to imatinib and sunitinib in gastrointestinal stromal tumor patients, Proc. Natl. Acad. Sci. U.S.A. 106 (2009) 1542–1547.

[37] G.A. Kaminski, R.A. Friesner, J. Tirado-Rives, W.L. Jorgensen, Evaluation and reparametrization of the OPLS-AA force field for proteins via comparison with accurate quantum chemical calculations on peptides, J. Phys. Chem. B 105 (2001) 6474–6487.

[38] Desmond Molecular Dynamics System, Version 2.2, D.E. Shaw Research/Schrödinger, LLC, New York, NY, 2009.

[39] K.J. Bowers, E. Chow, H. Xu, R.O. Dror, M.P. Eastwood, B.A. Gregersen, et al., Scalable algorithms for molecular dynamics simulations on commodity clusters, in: Proceedings of the 2006 ACM/IEEE Conference on Supercomputing, ACM, Tampa, FL, 2006, p. 84.

[40] MacroModel, Version 9.5, Schrödinger, LLC, New York, NY, 2007.

[41] W. Humphrey, A. Dalke, K. Schulten, VMD: visual molecular dynamics, J. Mol. Graph. 14 (1996) 33–38.

[42] K.K. Chohan, S.W. Paine, J. Mistry, P. Barton, A.M. Davis, A rapid computational filter for cytochrome P450 1A2 inhibition potential of compound libraries, J. Med. Chem. 48 (2005) 5154–5161.

[43] S. Lucas, R. Heim, C. Ries, K.E. Schewe, B. Birk, R.W. Hartmann, In vivo active aldosterone synthase inhibitors with improved selectivity: lead optimization providing a series of pyridine substituted 3,4-dihydro-1H-quinolin-2-one derivatives, J. Med. Chem. 51 (2008) 8077–8087.

[44] N. Lenkey, R. Karoly, P. Lukacs, E.S. Vizi, M. Sunesen, L. Fodor, A. Mike, Classification of drugs based on properties of sodium channel inhibition: a comparative automated patch-clamp study, PLoS ONE 5 (2010) e15568.

[45] M. Jalali-Heravi, M. Asadollahi-Baboli, A. Mani-Varnosfaderani, Shuffling multivariate adaptive regression splines and adaptive neuro-fuzzy inference system as tools for QSAR study of SARS inhibitors, J. Pharm. Biomed. Anal. 50 (2009) 853–860.

[46] M. Waldherr-Teschner, T. Goetze, J. Brickmann, MOLCAD computer aided visualisation and manipulation of models in molecular science, in: F.H. Post, A.J.S. Hin (Eds.), Proceeding of the Second Eurographics Workshop on Visualization in Scientific Computing, Delft, 1991.

[47] Prime, Version 2.1, Schrödinger, LLC, New York, NY, 2009.

[48] P.A. Kollman, I. Massova, C. Reyes, B. Kuhn, S. Huo, L. Chong, et al., Calculating structures and free energies of complex molecules: combining molecular mechanics and continuum models, Acc. Chem. Res. 33 (2011) 889–897.